西安交通大学
XI'AN JIAOTONG UNIVERSITY

World Scientific
www.worldscientific.com

Insulator-to-metal transition in $RCoO_3$ (R = Pr, Nd)

Sujoy Saha[*,¶], Sadhan Chanda[†], Alo Dutta[‡] and T. P. Sinha[§]

[*]Department of Materials Engineering, Indian Institute of Science
Bangalore 560012, Karnataka, India

[†]Department of Physics, Vivekananda College, East Udayrajpur
Madhyamgram, Kolkata 700129, West Bengal, India

[‡]Department of Condensed Matter Physics and Material Sciences
S. N. Bose National Centre for Basic Sciences, Block JD, Sector III
Salt Lake, Kolkata 700106, West Bengal, India

[§]Department of Physics, Bose Institute, 93/1 Acharya Prafulla Chandra Road
Kolkata 700009, West Bengal, India

[¶]sahasujoy3@gmail.com

We report a straightforward tool to investigate insulator-metal transition in $RCoO_3$ (R = Pr, and Nd) nanoparticles prepared by a sol–gel technique. Thermogravimetric analysis (TGA) of the as-prepared gel is performed to get the lowest possible calcination temperature of $RCoO_3$ nanoparticles. The Rietveld refinement of the powder X-ray diffraction (XRD) patterns for both samples shows that the samples crystallize in the orthorhombic (*Pnma*) phase at room temperature. The particle size of the sample is determined by scanning electron microscopy. Ac conductivity of the materials is analyzed in the temperature range from 303 K to 673 K and in the frequency range from 42 Hz to 1.1 MHz. The insulator-to-metal transition of $PrCoO_3$ and $NdCoO_3$ is analyzed by ac impedance spectroscopy. DC resistivity measurement is also done to cross check the insulator-metal transition in $RCoO_3$ system.

Keywords: Sol–gel technique; XRD; metal-insulator transition; transport property.

1. Introduction

The perovskite-type oxides RMO_3 (R = trivalent rare earth ion viz. La-Lu and M = 3d transition metal ion viz. Sc-Cu) are mainly insulating apart from a few compounds of M = Ni and Cu (e.g., $LaNiO_3$ and $LaCuO_3$).[1–3] In these compounds, the strong electron correlation of the 3d transition metal M is one of the reasons for the insulator-metal transition.[2] Among the RMO_3 perovskites, $RCoO_3$ shows a unique electronic phase change with change of temperature.[4] The most prominent example is $LaCoO_3$, which has been intensively studied.[5–9] The Co^{3+} ions in $LaCoO_3$ have a $3d^6$ configuration, which in principle can occur in three different spin states: nonmagnetic low-spin (LS: t_{2g}^6, e_g^0, $S = 0$), intermediate-spin (IS: t_{2g}^5, e_g^1, $S = 1$) or high-spin (HS: t_{2g}^4, e_g^2, $S = 2$). There is growing experimental and theoretical evidence that the first transition, occurring in $LaCoO_3$ between 50 K < T < 150 K, corresponds to a local excitation of LS Co^{3+} to a gradually enhanced HS state.[10–14] The second transition at $T \sim 500$ K is associated with an increase in the activation energy determined from a drastic change in the electrical conductivity, showing the metal-insulator transition ($T_{M–I}$), and it is currently attributed to the thermally activated mixture of LS/HS phase to a quasi-homogeneous phase of IS Co^{3+} states.[15–17] The same LS-(LS/HS)-IS scenario is applicable to rare earth $RCoO_3$ compounds, where both transition temperatures systematically increase and come close to each other with decreasing R ionic size.[18,19] It is generally agreed that the Co^{3+} ions realize the LS state at low temperatures. The energy levels of the Co^{3+} spin states are sensitive to the balance of intra-atomic exchange, crystal-field splitting, and covalency;[20] therefore, it can be expected that spin-state transitions can be tuned by external parameters such as pressure. The application of pressure should decrease the Co–O bond lengths, thereby increasing the crystal-field splitting and stabilizing the LS state, which should increase the spin-state transition temperature. Chemical pressure can be applied by replacing the La site with a smaller trivalent rare-earth ion (e.g., Pr and Nd).

To understand the spin state transition of $RCoO_3$ (R = Pr and Nd), different methods have been applied. Neutron diffraction techniques have been applied to understand the different spin states of $PrCoO_3$ and $NdCoO_3$.[21–23] Heat capacity of $RCoO_3$ is employed by Knížek *et al.*[21] to determine the proper reason for spin state transition. Transport properties of $PrCoO_3$ have been investigated by Tomeš *et al.*[24] Magnetism

[¶]Corresponding author.

and transport properties of $NdCoO_3$ have been studied by Fondado *et al.*[25] Raman spectroscopy studies of $RCoO_3$ have been investigated by Wei-Ran *et al.*[26] The seminal paper by Yamaguchi *et al.*[27] showcased systematic study of the metal-insulator transition of rare earth cobaltates crystals with the help of dc resistivity. It is interesting to note that the AC conductivity for a metal goes inversely to the frequency (*f*) of the ac field applied to the material, but for an insulator, the AC conductivity goes as $\sim f^n$ (where $0 < n < 1.0$). So, the conductivity study of a material with frequency will give an insight of the metallic and/or insulating character of a material. We can probe an insulator-to-metal transition by simply plotting the AC conductivity as a function of frequency. In this report, we have shown a simple approach to present the insulator-to-metal transition in polycrystalline $RCoO_3$ ($R =$ Nd and Pr) nanoparticles synthesized via sol–gel technique.

2. Experimental

The $RCoO_3$ nanoparticles were synthesized by a sol-gel method. $Pr(NO_3)_3$, $6H_2O$ (Alfa Aesar, 99.9%) or $Nd(NO_3)_3$, $6H_2O$ (Alfa Aesar, 99.9%), $Co(NO_3)_2$, $6H_2O$ (Merck, 99.5%) were separately dissolved in 20 ml deionized water with the stoichiometric ratio Pr/Co (Nd/Co) = 1/1. After being stirred for half an hour, praseodymium (neodymium) solution and cobalt solution were mixed. The resultant solution was transparent. A stable solution was then obtained by adding citric acid (Merck) separately dissolved in 20 ml of deionized water with a 1:1 molar ratio to the metal nitrates. After stirring for half an hour, ethylene glycol (Merck) with a 1:4 molar ratio with the metal nitrates was added. The precursor solution was stirred at 353 K for 6 h to form the sol. In order to synthesize $RCoO_3$ nanoparticles, the sol was dried to evaporate the liquid content, and a gelled mass was produced. The gel was heated until the auto-combustion was initiated. The dried gel was ground in an agate mortar. The ground gel was calcined in an alumina crucible at 973 K in the air for 4 h and brought to room temperature under controlled cooling with a cooling rate of 1 K/min. The calcined sample was compressed into a disc of thickness ~1.5 mm and diameter ~8 mm, using polyvinyl alcohol as a binder. Finally, the discs were sintered at 1023 K for 6 h and cooled down to room temperature by adjusting the cooling rate to 100 K/h. Thermogravimetric analysis (TGA) and differential scanning calorimetry were performed in order to determine the subsequent full crystallization of the as-prepared gel. TGA and DSC analysis were carried out in a TGA/DSC 1 (Mettler Toledo) instrument in the temperature range from 300 K to 1250 K at the heating rate of 10 K/min in the presence of nitrogen flow. The X-ray diffraction (XRD) patterns of calcined $RCoO_3$ powders were taken at room temperature by Rigaku–Miniflex II powder X-ray diffractometer using CuKα radiations in the 2θ range from 10º to 120º by step scanning at 0.02º per step. The Rietveld refinement of the XRD profile was performed using the Fullprof program.[28] Scanning electron micrographs of the samples were taken by

FEI Quanta 200 scanning electron microscope (SEM). The diffuse reflectance spectra of the samples were taken with Lamda 950 UV-VIS spectrometer. To measure the ac conductivity of $RCoO_3$, copper plates were used as electrodes. The AC conductance was measured in the frequency range from 42 Hz to 1.1 MHz and in the temperature range from 313 K to 673 K using an LCR meter (HIOKI-3250). The temperature was controlled by a programmable temperature controller (Eurotherm 818 P), and each measuring temperature was kept constant at measurement points with an accuracy of ±1 K, and data were collected while heating at a rate of 0.5 K−min−1. DC conductivity of the samples was measured by a Keithley 2400 SMU.

3. Results and Discussions

It is very crucial to determine the calcination temperature of the dried gel as at higher temperature, the coagulation of the nanoparticles tend to form grains with larger average grain size (~1 μm). Taking a small amount of the corresponding dried gels for $PrCoO_3$ and $NdCoO_3$, we carried out TGA. A large decrease (~50%) in the sample weight in the temperature range 550–700 K is associated with the elimination of bound water and organics[29,30] in the dried gel, Fig. 1. The large exothermic peak around 600–650 K in the DSC curve indicates crystallization of the cobaltates. In the later temperatures, 800–900 K, a slight decrease (~2%) in the TGA signal corresponds to the decomposition of oxycarbonates[31,32] also observed in similar materials. After 900 K, the TGA signal becomes parallel to the temperature axis giving the minimum temperature for processing the dried gel.
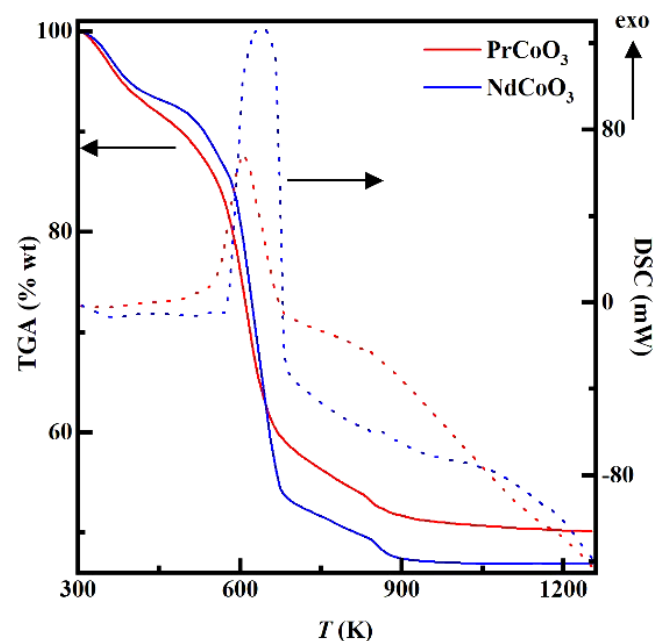

Fig. 1. Thermal analysis results for $RCoO_3$ ($R =$ Pr, Nd) precursor powder.
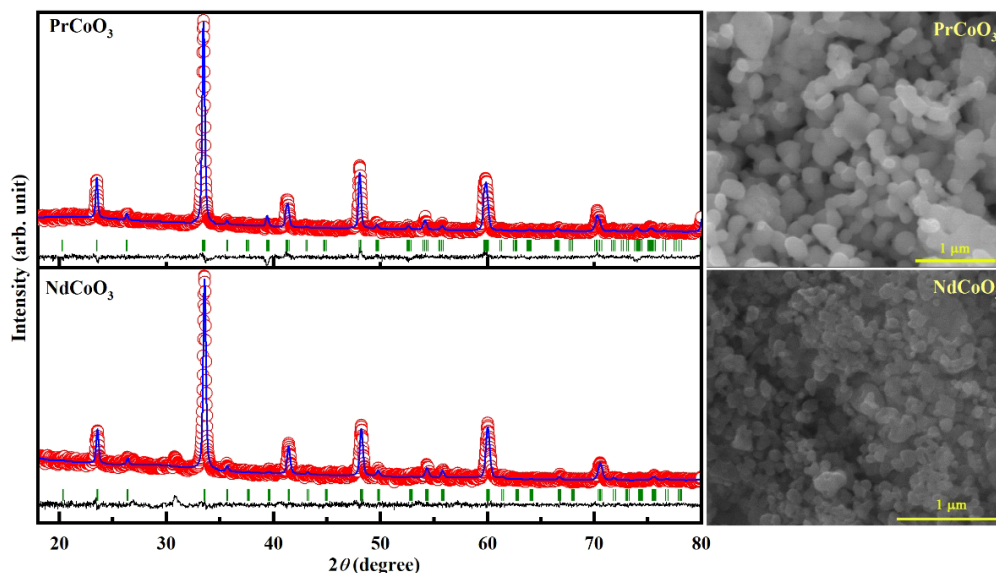
Fig. 2.   Rietveld plot of the room temperature XRD pattern of $RCoO_3$ (R = Pr, Nd). Open circles represent experimental data and the solid curve represents the calculated pattern. The vertical bar symbols indicate the Bragg positions and the bottom curve indicate the difference between the observed and the calculated patterns. The respective SEM images shown in the adjacent panes.

The phase formation after the calcification of the dried gels requires identification as low temperature calcification may lead towards untoward phase caused by the under-decomposed organometallic complex formed during the gel preparation.[33] In Fig. 2, we have shown the Rietveld fitted XRD diffraction patterns for $RCoO_3$ (R = Pr, Nd). We have tried to fit the observed patterns using the orthorhombic *Pnma* space group as reported earlier.[21,23,34] Apart from few unindexed peaks, all major peaks are well matched with the calculated pattern (blue curve, Fig. 2), indicating the phase formation of the materials. All the refinement parameters are tabulated in Table 1. The low reliability factors (R values) and low value of the goodness of fit (χ^2) indicates that the impurities are low in concentration.

The microstructural features of $RCoO_3$ (R = Pr, Nd) samples are represented by the corresponding SEM images given in the adjacent panes of the respective XRD patterns. The average particle size for both samples is found to be ~50±4 nm. The near homogeneous distribution of the nanoparticles for both systems indicates the undisrupted transport of the charge carriers through the materials. The grain-to-grain transfer of the charge carriers is also unaltered throughout the system, as charge carriers do not experience any variation of potential barriers created by grain boundaries. A significantly less number of voids also eliminates the chances of spurious conductivity.

The discussion about the insulator-metal transition of any material seems incomplete without prior knowledge about the optical bandgap of the material. To plug the lacuna, we have taken the reflectivity data of the materials at room temperature and converted them into the Kubelka–Munk function ($F(R_\infty)$). The bandgap energy of the material is related

with the into Kubelka–Munk function, similar to the relation proposed by Tauc, Davis, and Mott.[35–37] After inserting the Kubelka–Munk function into the Tauc relation, the final expression reads as

$$(F(R_\infty)h\nu)^{1/n} = A(h\nu - E_g), \qquad (1)$$

where h = Planck's constant, ν = frequency of vibration, E_g = band gap, A = proportional constant independent of the photon energy.[35–37] The values of n for direct allowed and indirect allowed transitions are 1/2 and 2, respectively. Using this relation, a graph is plotted between $(F(R_\infty)h\nu)^2$ taking $n = 1/2$ and energy $h\nu$ as shown in Fig. 3. The extrapolation of the linear absorption-edge part of this graph with a straight line to $(F(R_\infty)h\nu)^2 = 0$ axis gives the value of the direct bandgap. The values of the optical band gaps of PCO and NCO for direct transition are found to be ~1.7 eV. It is to be noted that both materials show significant absorption even in the sub-bandgap energy, so the direct estimation of the bandgap with the Tauc relation is critical.[38] The estimated gap of the materials is in good agreement with the earlier reports.[27]

3.4.   *Electrical properties*

If one assumes that all the dielectric loss in the temperature range studied (303–673 K) is due to the conductivity of the materials, then the AC conductivity can be expressed as $\sigma_{ac}(\omega) = \varepsilon''(\omega)\varepsilon_0\omega$, here, σ_{ac} is the real part of the conductivity and ε'' is the imaginary part of complex dielectric constant (ε^*). Figure 4 shows the log-log plot of the frequency dependent AC conductivity of $RCoO_3$ (R = Pr and Nd)

Table 1. Details of the structure refinement of $RCoO_3$ (R = Pr, Nd).

Sample	Atom	Wyckoff	Site symmetry	x	y	Z	B_{iso} (Å²)
				a = 5.3373 (5), b = 7.5714(8), c = 5.3713(5)			
	Pr	4c	C_s^{xy}	0.0270 (5)	0.25	0.0149 (5)	0.625
	Co	4b	C_i	0	0	0.5	0.420
PrCoO₃	O$_I$	4c	C_s^{xy}	0.4955(64)	0.25	−0.0548 (85)	0.161
	O$_{II}$	8d	C_1	0.2598(70)	0.0548(31)	0.7503(79)	0.362

Bond angle (°)
Co–O$_I$–Co = 162.2
Co–O$_{II}$–Co = 155.1
Tilt angle (°)
$\theta_x = \theta_z = 12.45, \theta_y = 8.9$

Reliability factors
R_p = 3.01, R_{wp} = 4.00,
R_{exp} = 3.84, χ^2 = 1.09

Sample	Atom	Wyckoff	Site symmetry	x	y	Z	B_{iso}
				a = 5.3367(7), b = 7.5444(19), c = 5.3457(16)			
	Nd	4c	C_s^{xy}	0.0330(5)	0.25	0.0059(15)	0.364
	Co	4b	C_i	0	0	0.5	0.119
NdCoO₃	O$_I$	4c	C_s^{xy}	0.4903(59)	0.25	−0.0667(20)	0.201
	O$_{II}$	8d	C_1	0.2738(96)	0.0324(86)	0.7008(95)	0.555

Bond angle (°)
Co–O$_I$–Co = 158.3
Co–O$_{II}$–Co = 158.0
Tilt angle (°)
$\theta_x = \theta_z = 11.0, \theta_y = 10.85$

Reliability factors
R_p = 2.69, R_{wp} = 3.48,
R_{exp} = 3.87, χ^2 = 0.805

nanoparticles in the temperature range from 303 K to 673 K. For both the materials, we observe a frequency independent plateau region below 150 kHz at all observed temperatures. At low frequency (< 150 kHz), the ac conductivity is found to be frequency independent due to the nonequilibrium occupancy of the trapped charges.[38] and the conductivity is approximately equal to the dc value. In this region conduction mechanism is the same as that for DC conduction which is the hopping of charged particles from one localized site to another. The cations surrounded by close-packed oxygen anions can be treated as isolated from each other due to little direct overlap of the charge clouds. This localization gives rise to the formation of the polaron, and the charge transport may be considered between the nearest neighbor sites. Above 150 kHz the AC conductivity for both materials shows dispersion. As the frequency is increased, the occupancy of the trap centers is reduced by making them available for conduction. It facilitates the conductive state to become more active by promoting the hopping of electrons and holes. In the low temperature range the conductivity for both materials begins to increase nonlinearly after the frequency exceeds the critical frequency (ω_H) since the capacitor admittance becomes numerically larger than the resistor admittance with increasing frequency. The AC conductivity spectra for both materials can be fitted with Jonscher's power[39] law given by

$$\sigma_{ac} = \sigma_{dc}\left[1+\left(\frac{\omega}{\omega_H}\right)^n\right], \qquad (3)$$

where σ_{dc} = DC conductivity as obtained from the extrapolation towards the lower frequency side. The exponent n varies from 0 to 1. The fitting parameters are listed in Table 2.

In the low temperature range the materials show a lower conductivity which increases after a critical frequency ($\omega_H = 2\pi\nu_H$), showing a typical insulating behavior. The decrease of the AC conductivity for both materials at higher frequencies (>150 kHz) in the higher temperatures indicates a metallic behavior.[40] Hence, there is an insulator-metal transition in these samples similar to the earlier report.[27]

To visualize the variation of the conductivity with temperature we have plotted the conductivity for PCO and NCO in Fig. 5. At 1.1 MHz both PCO and NCO show a peak around ~525 K. It is quite contrasting with the results by Yamaguchi et al.[27] wherein the insulator-metal transition temperatures
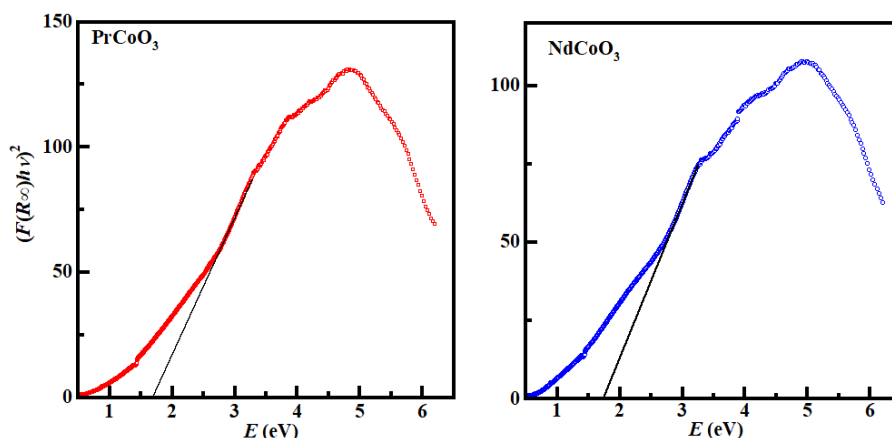
Fig. 3. Modified Kubelka–Munk function plot for $RCoO_3$ (R = Pr and Nd).
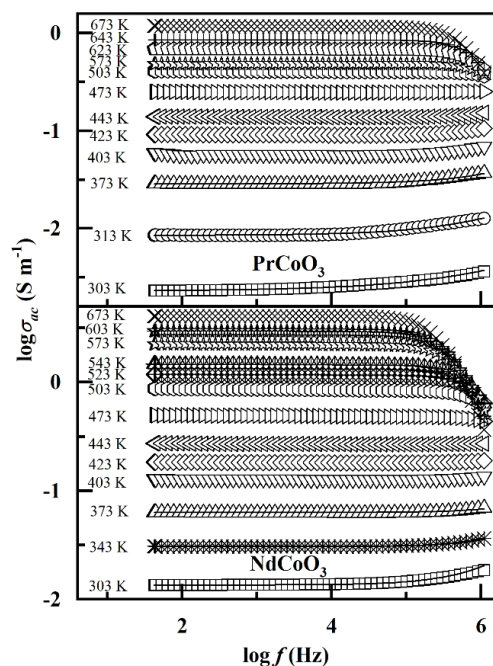
Fig. 4.   AC conductivity spectra of $RCoO_3$ (R = Pr and Nd).

Table 2.   Fitting parameters for the conductivity spectra of $RCoO_3$ (R = Pr, Nd).

Sample	Temperature (K)	σ_{dc} (mS m^{-1})	ν_H (kHz)	n
PrCoO$_3$	303	2.291	3500	0.4
	313	8.472	3980	0.52
	473	28.576	7958	0.64
NdCoO$_3$	303	13.521	2547	0.8
	343	30.620	7958	0.9
	373	63.096	14,324	0.95

(T_{I-M}) for PCO and NCO are different with $T_{I-M, \text{NCO}}$ occurring at higher temperature. The cause of this discrepancy is the quality of the materials under investigation. We have prepared nanocrystalline ceramics with some impurities, whereas Yamaguchi *et al.*[27] used good quality single crystals. Yamaguchi *et al.*[27] have also mentioned that the systematic variation of their data was due to the quality of their prepared crystals. Our intention is to introduce a simple experimental procedure to visualize the *I–M* transition in $RCoO_3$ type materials; hence, the merging of the T_{I-M} for PCO and NCO can be overlooked as far as the phenomenon is only concerned. Nevertheless, we can explain the merger of T_{I-M} for PCO and NCO. The *I–M* transition for narrow gap semiconductors is ruled out due to the large band gap (~1.7 eV) of these materials. Now due to the nanocrystalline nature of the samples, the probability of charge transfer excitations to the Co-e_g band from the bonding and antibonding states consisting of Co-t_{2g} and O-2p states becomes comparable, giving rise to the same T_{I-M}.
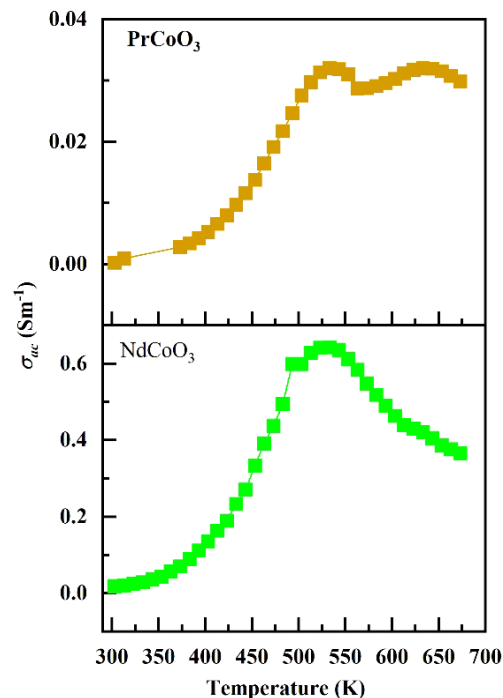
Fig. 5.   Temperature dependence of the AC conductivity (σ_{ac}) of $RCoO_3$ (R = Pr and Nd).
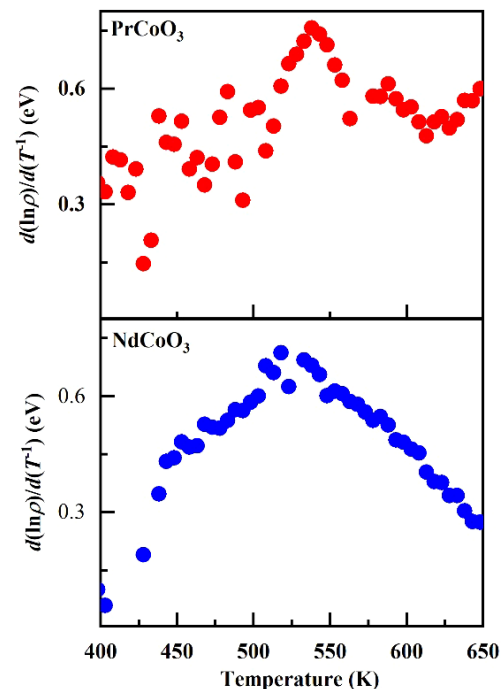
Fig. 6.   Temperature dependence of the DC conductivity (σ_{dc}) of $RCoO_3$ (R = Pr and Nd).

The representation of the insulator-metal transition in $RCoO_3$ materials using ac conductivity approach discussed above is simple. Nevertheless, the transport dynamics with an ac perturbation is more complex as compared to a dc

conductivity approach. To have a complete and counter validation of the insulator metal transition in the RCoO$_3$ samples we have also studied the conventional dc conductivity. In Fig. 6, we have plotted resistivity (ρ) in terms of a quantity $d(\ln\rho)/d(T^{-1})$ as a function of temperature (T) for RCoO$_3$ samples. The quantity $d(\ln\rho)/d(T^{-1})$ represents the activation energy in the case of thermally activated conduction.[27] The insulator-metal transition for both the samples is ~530 K close to the value obtained from ac conductivity.

4. Conclusions

RCoO$_3$ (R = Pr, Nd) nanoparticles synthesized by a sol–gel route have been characterized by TGA. TGA of the as-prepared gels indicates that the lowest possible calcination temperature of the RCoO$_3$ nanoparticles is 973 K. Rietveld refinement of the XRD data of the calcined samples shows that both the samples crystallize with orthorhombic *Pnma* space group. The value of the optical band gap for both samples is found to be ~1.70 eV. The AC conductance of the materials measured in the frequency range from 42 Hz to 1.1 MHz and in the temperature range from 313 K to 673 K shows *I–M* transition. Insulator-to-metal transition temperature for PrCoO$_3$ and NdCoO$_3$ is found to be ~525 K from ac conductivity studies. DC conductivity measurements show an insulator-to-metal transition temperature ~530 K.

References

[1]C. N. R. Rao and G. V. S. Rao, Electrical conduction in metal oxides, *Phys. Status Solidi A* **1**, 597 (1970).

[2]T. Arima, Y. Tokura and J. B. Torrance, Variation of optical gaps in perovskite-type 3d transition-metal oxides, *Phys. Rev. B* **48**, 17006 (1993).

[3]I. Solovyev, N. Hamada and K. Terakura, Variation of optical gaps in perovskite-type 3d transition-metal oxides, *Phys. Rev. B* **53**, 7158 (1996).

[4]G. Thornton, B. C. Tofield and A. W. Hewat, A neutron diffraction study of LaCoO$_3$ in the temperature range 4.2 < *T* < 1248 K, *J. Solid State Chem.* **61**, 301 (1986).

[5]G. H. Jonker and J. H. van Santen, Magnetic compounds with perovskite structure III: Ferromagnetic compounds of cobalt, *Physica* **19**, 120 (1953).

[6]J. B. Goodenough and P. M. Raccah, Complex vs band formation in Perovskite oxides, *J. Appl. Phys.* **36**, 1031 (1965).

[7]M. A. Señarís-Rodríguez and J. B. Goodenough, LaCoO$_3$ revisited, *J. Solid State Chem.* **116**, 224 (1995).

[8]T. Saitoh, T. Mizokawa, A. Fujimori, M. Abbate, Y. Takeda and M. Takano, Electronic structure and temperature-induced paramagnetism in LaCoO$_3$, *Phys. Rev. B* **5**, 4257 (1997).

[9]K. Asai, A. Yoneda, O. Yokokura, J. M. Tranquada, G. Shirane and K. Kohn, Two spin-state transitions in LaCoO$_3$, *J. Phys. Soc. Jpn.* **67**, 290 (1998).

[10]S. Noguchi, S. Kawamata, K. Okuda, H. Nojiri and M. Motokawa, Evidence for the excited triplet of Co^{3+} in LaCoO$_3$, *Phys. Rev. B* **66**, 94404 (2002).

[11]Z. Ropka and R. J. Radwanski, ^{5}D term origin of the excited triplet in LaCoO$_3$, *Phys. Rev. B* **67**, 172401 (2003).

[12]M. W. Haverkort, Z. Hu, J. C. Cezar, T. Burnus, H. Hartmann, M. Reuther, C. Zobel, T. Lorenz, A. Tanaka, N. B. Brookes, H. H. Hsieh, H.-J. Lin, C. T. Chen and L. H. Tjeng, Spin state transition in LaCoO$_3$ studied using soft X-ray absorption spectroscopy and magnetic circular dichroism, *Phys. Rev. Lett.* **97**, 176405 (2006).

[13]A. Podlesnyak, S. Streule, J. Mesot, M. Medarde, E. Pomjakushina, K. Conder, A. Tanaka, M. W. Haverkort and D. I. Khomskii, Spin-state transition in LaCoO$_3$: Direct neutron spectroscopic evidence of excited magnetic states, *Phys. Rev. Lett.* **97**, 247208 (2006).

[14]K. Knížek, Z. Jirák, J. Hejtmánek and P. Novák, Character of the excited state of the Co^{3+} ion in LaCoO$_3$, *J. Phys.: Condens. Matter* **18**, 3285 (2006).

[15]T. Kyômen, Y. Asaka and M. Itoh, Thermodynamical analysis of spin-state transitions in LaCoO$_3$: Negative energy of mixing to assist thermal excitation to the high-spin excited state *Phys. Rev. B* **71**, 024418 (2005).

[16]Z. Jirák, J. Hejtmánek, K. Knížek and M. Veverka, Electrical resistivity and thermopower measurements of the hole- and electron-doped cobaltites, *Phys. Rev. B* **78**, 014432 (2008).

[17]K. Knížek, Z. Jirák, J. Hejtmánek, P. Novák and W. Ku, GGA+U calculations of correlated spin excitations in LaCoO$_3$, *Phys. Rev. B* **79**, 014430 (2009).

[18]K. Knížek, Z. Jirák, J. Hejtmánek, M. Veverka, M. Maryško, G. Maris and T. T. M. Palstra, Structural anomalies associated with the electronic and spin transitions in LnCoO$_3$, *Eur. Phys. J. B* **47**, 213 (2005).

[19]K. Knížek, Z. Jirák, J. Hejtmánek, P. Henry and G. André, Structural anomalies, spin transitions, and charge disproportionation in LnCoO$_3$, *J. Appl. Phys.* **103**, 07B703 (2008).

[20]M. A. Korotin, S. Y. Ezhov, I. V. Solovyev, V. I. Anisimov, D. I. Khomskii and G. A. Sawatzky, Intermediate-spin state and properties of LaCoO$_3$, *Phys. Rev. B* **54**, 5309 (1996).

[21]K. Knížek, J. Hejtmánek, Z. Jirák, P. Tomeš, P. Henry and G. André, Neutron diffraction and heat capacity studies of PrCoO$_3$ and NdCoO$_3$, *Phys. Rev. B* **79**, 134103 (2009).

[22]J. Yu, D. Phelan and D. Louca, Spin-state transitions in PrCoO$_3$ investigated by neutron scattering, *Phys. Rev. B* **84**, 132410 (2011).

[22]Y. Ren, J.-Q. Yan, J.-S. Zhou, J. B. Goodenough, J. D. Jorgensen, S. Short, H. Kim, Th. Proffen, S. Chang and R. J. McQueeney, Spin-state transitions in PrCoO$_3$ studied with neutron powder diffraction, *Phys. Rev. B* **84**, 214409 (2011).

[24]P. Tomeš, M. H. Aguirre, R. Robert, A. Shkabko, E. H. Otal and A. Weidenkaff, Transport and magnetic properties of PrCo$_{1−x}$Ni$_x$O$_3$ (x = 0.0–0.7), *J. Phys. D: Appl. Phys.* **44**, 305402 (2011).

[25]A. Fondadoa, M. P. Breijo, C. Rey-Cabezudo M. Sánchez-Andújar, J. Mira, J. Rivas and M.A. Señarís-Rodríguez, Synthesis, characterization, magnetism and transport properties of Nd1-xSrxCoO$_3$ perovskites, *J. Alloy Compd.* **323**–**324**, 444 (2001).

[26]W. Wei-Ran, X. Da-Peng, S. Wen-Hui, D. Zhan-Hui, X. Yan-Feng and S. Geng-Xin, Raman active phonons in RCoO$_3$ (R = La, Ce, Pr, Nd, Sm, Eu, Gd, and Dy) perovskites, *Phys. Lett.* **22**, 2400 (2005).

[27]S. Yamaguchi, Y. Okimoto and Y. Tokura, Bandwidth dependence of insulator-metal transitions in perovskite cobalt oxides, *Phys. Rev. B* **54**, R11022 (1996).

[28]J. Rodrigues-Carvajal, FullProf, A Rietveld Refinement and Pattern Matching Analysis Program (Laboratories Leon Brillouin [CEA-CNRS], France, 2000).

[29]H. Shen, G. F. Cheng, A. H. Wu, J. Y. Xu and J. T. Zhao, Combustion synthesis and characterization of nano-crystalline $LaFeO_3$ powder, *Phys. Status Solidi A* **206**, 1420 (2009).

[30]J. Chandradass and K. H. Kim, Nano-$LaFeO_3$ powder preparation by calcining an emulsion precursor, *Mater. Chem. Phys*. **122**, 329 (2010).

[31]X. Li, C. Tang, M. Ai, L. Dong and Z. Xu, Controllable synthesis of pure-phase rare-earth orthoferrites hollow spheres with a porous shell and their catalytic performance for the CO+ NO reaction, *Chem. Mater*. **22**, 4879 (2010).

[32]L. Ju, Z. Chen, L. Fang, W. Dong, F. Zheng and M. Shen, Sol-gel synthesis and photo-fenton-like catalytic activity of $EuFeO_3$ nanoparticles, *J. Am. Ceram. Soc*. **94**, 3418 (2011).

[33]S. Saha, S. Chanda, A. Dutta and T. P. Sinha, Dielectric relaxation and phonon modes of $NdCrO_3$ nanostructure, *J. Sol-Gel Sci. Technol*. **69**, 553–563 (2014).

[34]C. Tealdi, L. Malavasi, F. Gozzo, C. Ritter, M. C. Mozzati, G. Chiodelli and G. Flor, Correlation between transport properties and lattice effects in the $NdCoO_3$-based catalysts and sensor materials, *Chem. Mater*. **19**, 4741–4750 (2007).

[35]J. Tauc, *Optical Properties of Solids* (Plenum, New York, 1969).

[36]E. A. Davis and N. F. Mott, Conduction in non-crystalline systems V. Conductivity, optical absorption and photoconductivity in amorphous semiconductors, *Philos. Mag*. **22**, 903 (1970).

[36]N. F. Mott and E. A. Davis, *Electronic Processes in Noncrystalline Materials* (Clarendon, Oxford, 1979).

[38]P. Makuła, M. Pacia and W. Macyk, How to correctly determine the band gap energy of modified semiconductor photocatalysts based on UV-Vis spectra, *J. Phys. Chem. Lett*. *9*, 6814–6817 **(2018).**

[39]A. K. Jonscher, *Dielectric Relaxation in Solids* (Chelsea Dielectric Press, London, 1996).

[40]N. W. Ashcroft and N. D. Mermin, *Solid State Physics* (Cengage Learning, New York, 2011).